Reduction of in-plane field required for spin-orbit torque magnetization reversal by insertion of Au spacer in Pt/Au/Co/Ni/Co/Ta

M. Mann, and G. S. D. Beach

Citation: APL Materials **5**, 106104 (2017); doi: 10.1063/1.4991950
View online: https://doi.org/10.1063/1.4991950
View Table of Contents: http://aip.scitation.org/toc/apm/5/10
Published by the American Institute of Physics

APL MATERIALS **5**, 106104 (2017)

Reduction of in-plane field required for spin-orbit torque magnetization reversal by insertion of Au spacer in Pt/Au/Co/Ni/Co/Ta

M. Mann and G. S. D. Beach[a]
Department of Materials Science and Engineering, Massachusetts Institute of Technology, Cambridge, Massachusetts 02139, USA

(Received 24 June 2017; accepted 13 September 2017; published online 12 October 2017)

Spin-orbit torques and current-induced switching are studied in perpendicularly magnetized Pt/Au/(Co/Ni/Co) films as a function of Au insertion layer thickness t_{Au}. By simultaneously varying the ferromagnet layer thickness, a parametric series of samples with nearly constant anisotropy were prepared. On this series, spin orbit torques were characterized by harmonic voltage and hysteresis loop shift measurements, and current-induced switching was examined as a function of the in-plane bias field. Little variation is seen for $t_{Au} < 0.5$ nm, whereas for $t_{Au} > 0.5$ nm, a series of well-correlated effects appear. Both the loop shift efficiency and the Slonczewski-like spin-orbit torque effective field double, while the in-plane field required to saturate the loop shift efficiency decreases by a factor of ~10. Correspondingly, the current and in-plane field required for spin-orbit torque switching are reduced by about 90%. These results suggest that a thin Au insertion layer reduces the Dzyaloshinskii-Moriya interaction strength and improves spin transmission at the spin Hall metal/ferromagnet interface, substantially reducing the in-plane field and currents for spin orbit torque switching. https://doi.org/10.1063/1.4991950

Electrical currents flowing through heavy-metal/ferromagnetic (HM/FM) heterostructures exhibiting large spin-orbit coupling produce spin-orbit torques (SOTs) on the magnetization of the ferromagnetic layer via the spin Hall effect[1–4] and the Rashba-Edelstein effect.[5–7] The SOT is composed of a field-like and a Slonczewski-like torque. In particular, the Slonczewski-like torque can drive perpendicular magnetization reversal, potentially enabling low-power memory and logic spintronic devices.[2,5,8] However, deterministic SOT switching of materials with perpendicular magnetic anisotropy (PMA) requires an in-plane bias field, which is undesirable for applications. Several mechanisms have been recently proposed to engineer built-in bias fields to replace the usual externally applied field, including exchange bias[9–11] and stray fields from thick adjacent magnetic layers.[12] However, achieving large in-plane bias fields is difficult, and degradation can occur, e.g., through Joule heating and exchange bias training effects,[13] reducing the reliability of such schemes.

On the other hand, little work has been done to reduce the magnitude of the bias field needed for switching, which could place less stringent requirements on the bias field source. In the single domain switching picture, the in-plane field [H_{long}, see Fig. 1(b)] is applied to tilt the magnetization along the current flow direction. This leads to an out-of-plane component of the Slonczewski-like effective field, proportional to the projection of the magnetization along the current axis that can switch the easy axis magnetization. In this case, the H_{long} required to achieve switching at a given current density should scale with the anisotropy field, since the latter determines the magnetization tilt angle. But since large PMA is needed for thermal stability, it would seem difficult to significantly decrease the needed H_{long} magnitude.

[a]Author to whom correspondence should be addressed: gbeach@mit.edu.

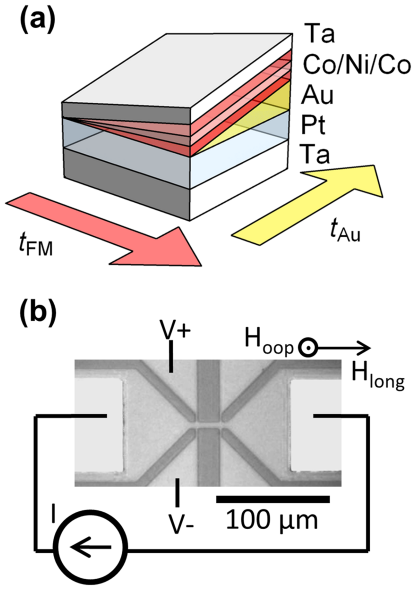

FIG. 1. (a) Schematic of a dual wedge structure sample. (b) Optical micrograph and schematic electrical connections for patterned Hall bars.

In contrast to the single-domain picture, Lee *et al.*[14] and Pai *et al.*[15] have shown that SOT driven magnetization switching is nonuniform and occurs by domain nucleation and domain wall propagation. Current-driven expansion of reversed domains by the Slonczewski-like torque can occur only if H_{long} overcomes the domain wall chirality set by the Dzyaloshinskii-Moriya interaction (DMI) so that adjacent domain walls propagate in opposite directions. The bilayer systems that exhibit large SOTs also typically show strong interfacial DMI, requiring large H_{long} for SOT switching. To reduce the required field, it is hence desirable to independently control the interfacial DMI and SOT, minimizing the former, while maximizing the latter. Hence, SOT switching efficiency could presumably be enhanced by insertion of a spacer layer at the HM/FM interface that reduces the DMI while remaining transparent to spin injection.

In this letter, we systematically examine SOTs and current-induced switching in Pt/Au/ferromagnet heterostructures as a function of the thickness of the Au insertion layer. We find that at Au thicknesses greater than ~0.5 nm, the DMI is substantially reduced, dropping by about an order of magnitude for ~0.8 nm of Au. At the same time, the Au layer enhances spin transmission and modulates the SOT effective field toward a more Slonczewski-like character. The utility of these effects is confirmed with direct switching measurements that show a reduction of H_{long} and current required to reverse the magnetization by a factor of ~10. These results are important both for technological applications and as a demonstration that DMI and SOT can be engineered independently.

We grew a series of Ta(3)/Pt(3)/Au(t_{Au})/(Co/Ni/Co) (t_{FM})/Ta(1) films (numbers in parentheses indicate nominal thicknesses in nm; Co, Ni, and Co layer thicknesses were equal) by dc-magnetron sputtering on a thermally oxidized Si substrate to produce the structure shown in Fig. 1(a). We used deposition source masks to independently vary t_{Au} and t_{FM} along orthogonal directions in a double-wedge geometry, spanning 0-2.4 nm for t_{Au} and 0.9-1.6 nm for t_{FM} over a distance of about 20 mm. The bottom Ta layer was used for adhesion and the top Ta layer, nominally fully oxidized, served as a protective cap. We precalibrated the deposition rate as a function of position for the two wedges by profilometry. Hall bars (32 μm × 6 μm with two 3 μm wide crossbars) were fabricated by standard photolithography and lift-off methods, patterned as a dense array across the wedge. A photomicrograph of a patterned device, annotated with the generalized electrical measurement configuration, is shown in Fig. 1(b).

Magnetic properties were characterized as a function of t_{Au} and t_{FM} from hysteresis loops measured on Hall crosses at fixed spatial intervals on the wedge, via the anomalous Hall effect (AHE)

using a standard lock-in technique. The coercivity H_c was determined from out-of-plane hysteresis loops, and the perpendicular anisotropy field H_k was determined from a Stoner-Wohlfarth fit of the curvature of the AHE signal versus in-plane field. Figures 2(a) and 2(b) show maps of H_c and H_k, respectively, which both decrease with increasing t_{Au} and t_{FM}. From these data, we identified a series of devices [solid symbols in Figs. 2(a) and 2(b)] with t_{Au} spanning a range ~0-0.8 nm, where t_{FM} also varies such that H_k was nearly constant [Fig. 2(c)]. We identify samples with constant H_k to control the magnetization tilt angle resulting from a given in-plane field, allowing a fair comparison of the FM response to SOT. Here, H_k ranges between 4.5 and 4.7 kOe, except for t_{Au} = 0.81 nm, for which H_k = 3.8 kOe. At larger t_{Au}, the ferromagnet magnetizes in-plane, placing an upper limit on gold thickness in the subsequent measurement series. Subsequent measurements focus on this set of devices so that the effect of t_{Au} can be probed independent of variations in H_k.

The Slonczewski-like (H_{SL}) and field-like (H_{FL}) SOT effective fields were obtained by performing standard field-swept first- and second-harmonic AHE measurements as described elsewhere,[16] corrected for the planar Hall effect.[17] As seen in Fig. 2(d), H_{SL} changes little below t_{Au} = 0.5 nm but increases significantly as t_{Au} increases to 0.81 nm nominal thickness. At the same time, the ratio H_{SL}/H_{FL} increases, indicating that the spin-orbit torque becomes more Slonczewski-like in character. The Slonczewski-like spin torque efficiency ξ_{SL} was calculated according to Ref. 18 $H_{SL} = \hbar\xi_{SH}|j_e|/(2|e|M_s t_{FM})$, where j_e is the charge current density, e is the electron charge, and M_s is the saturation magnetization.[8] Zhang *et al.* and Hai *et al.* indicate that a magnetic dead layer does not form at sputtered Pt/Co or Au/Co interfaces, so we assume bulk values for M_s.[19,20] Here, j_e in the Pt layer was estimated using a parallel resistor model. We find $\xi_{SL} \approx 0.16$ in the low t_{Au} regime, in close agreement with Pai *et al.*[18] and Woo *et al.*,[21] whereas at thicker t_{Au}, we find a significant increase in ξ_{SL}. ξ_{SL} is related to the internal spin Hall angle θ_{SH} of Pt and the interfacial spin transparency T_{int} through[18] $\xi_{SL} = \theta_{SH} T_{int}$. These results hence suggest that spin transmission, which is related to the interfacial spin-mixing conductance,[18] is enhanced by the Au insertion layer. Similar

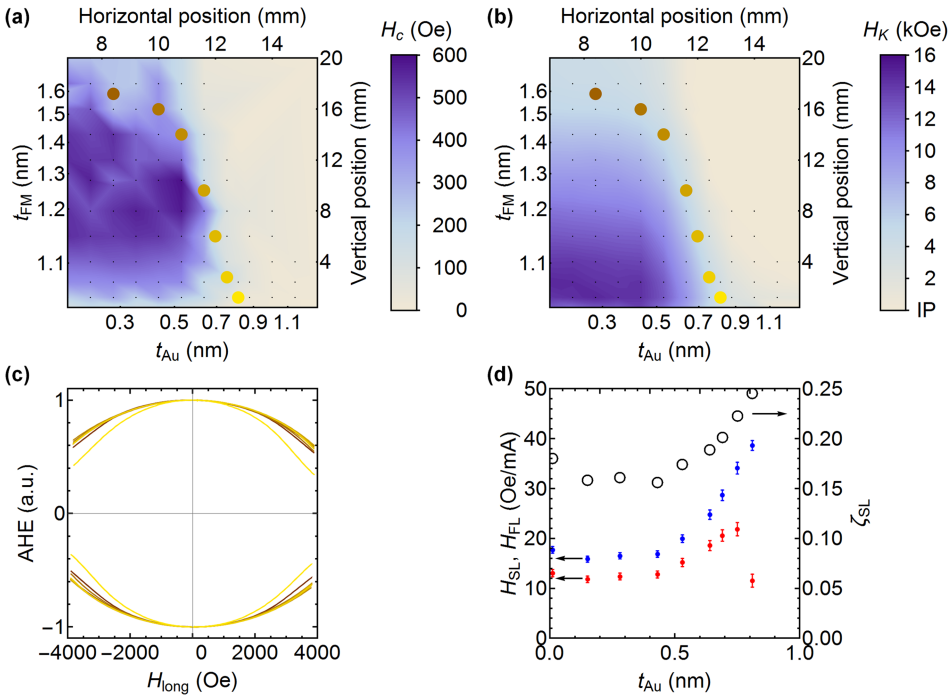

FIG. 2. (a) Coercivity (H_c) map of the dual wedge structure, plotted versus position on wedge (top, right axes) and calibrated layer thicknesses (left, bottom axes). Small black points indicate locations where measurements were taken. (b) Corresponding map for the perpendicular anisotropy field H_k. Filled circles indicate the sample set with nearly constant anisotropy, color-coded to match plots in Figs. 2(c), 3(c), and 4(c). (c) Normalized first harmonic anomalous Hall effect (AHE) voltage versus in-plane field for the nearly constant anisotropy sample set. (d) Effective spin-orbit torque fields, H_{SL} (blue) and H_{FL} (red), and Slonczewski-like spin torque efficiency (ξ_{SL}) (open circles) versus t_{Au}.

spin transmission enhancement by interlayer insertion has previously been observed,[22–27] and one can reasonably expect an enhancement in ξ_{SL} by appropriate choice of interface material since the "internal" spin Hall angle for Pt is expected to be 0.30 or greater, whereas the apparent value after spin backflow and spin memory loss can appear closer to 0.07 in Pt/Co.[18]

Alternatively, the increased spin torque could be explained by greater spin generation by the Rashba effect at the interface. Because both the Rashba effect and the spin Hall effect can both produce the same torques,[15] they cannot be distinguished in this case.

Hysteresis loop shift measurements were performed to confirm the enhanced spin torque efficiency and probe the DMI strength and its variation with t_{Au}. The method, as described by Pai *et al.*,[15] consists of measuring out of plane hysteresis loops under DC H_{long} and DC in-plane currents. The loops shift to the left or right in proportion to the out-of-plane component of the Slonczewski-like current-induced effective field, as the SOT modulates the domain wall depinning [Fig. 3(a)]. H_{long} adds opposite Zeeman energy terms to opposing homochiral domain walls; thus, it changes the relative velocity of up-down and down-up domain walls. At a critical H_{long} related to the DMI effective field, one domain wall will reverse chirality and propagation direction. This is observed as a critical field H_{sat} above which the loop shift efficiency saturates since the magnitude of the current-induced effective field in the domain walls is maximized when their moments are all aligned parallel or antiparallel to the current-flow direction.[15]

Figure 3(a) shows an exemplary out-of-plane hysteresis loop under positive H_{long} for two opposite-polarity currents, which result in opposite horizontal shifts of the loop center. The positions of the left and right zero crossings and the loop shift are plotted in Fig. 3(b) versus current. The loop-shift efficiency χ, taken as the slope of the loop shift versus current, is plotted in Fig. 3(c) versus the in-plane longitudinal field for the set of nearly constant anisotropy samples. As expected, a nearly zero loop shift is observable when zero H_{long} is applied. A nonzero H_{long} sets the magnitude and sign of the loop shift efficiency, up to a critical point where increasing the magnitude of H_{long} produces no further increases in shift efficiency, which is expected to correspond to the DMI effective field. On the sample with direct Pt/Co contact, H_{sat} = 1100 Oe, close but somewhat smaller than that reported

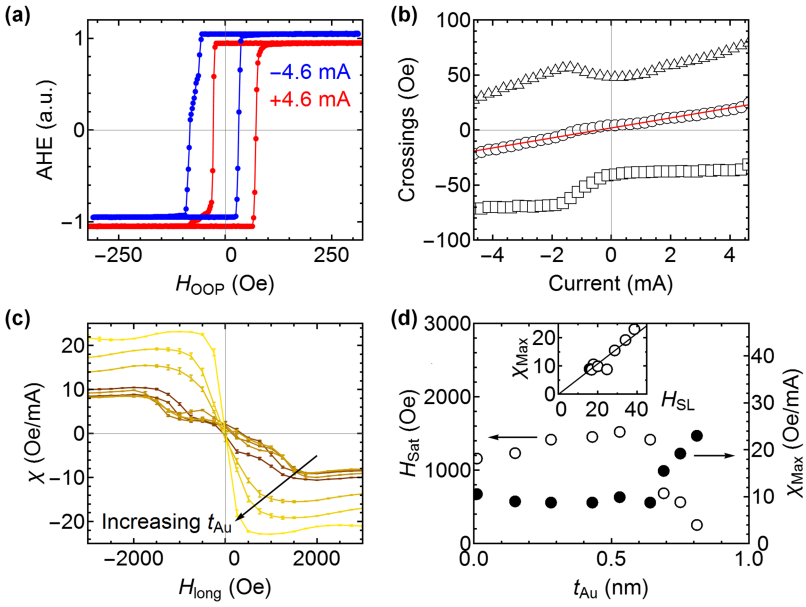

FIG. 3. (a) Exemplary normalized anomalous Hall effect (AHE) out-of-plane hysteresis loops measured under H_{long} = 250 Oe and in-plane currents of opposite sign. Loops displaced vertically for clarity. (b) Hysteresis loop shift, visualized as the mean (circles) between the left (squares) and right (triangles) zero crossings, versus current. Solid line is a linear fit. (c) Loop shift efficiency versus in-plane field for a set of nearly constant anisotropy samples. Error bars represent the standard deviation of the slope of linear fits of the loop shift versus current. (d) Saturation field H_{sat} (empty circles) taken as position of knee in (c), and maximum loop shift efficiency $H_{\mathrm{Eff\_Max}}$ (filled circles) versus t_{Au} for the nearly constant anisotropy sample set. Inset shows linear relationship between $H_{\mathrm{Eff\_Max}}$ and H_{SL} from harmonic torque measurements.

by Pai *et al.*[15] and Emori *et al.*[28] H_{sat} is constant or slightly increasing for t_{Au} less than 0.5 nm, then decreases by 90% as t_{Au} increases to 0.81 nm. This observation is consistent with a model where the interfacial DMI from the Pt/Co interface is attenuated as the contact is increasingly occluded by the gold spacer. At the same time as H_{sat} decreases, the maximum shift efficiency χ_{max} increases and appears correlated with H_{SL} [Fig. 3(d), inset]. The combination of large shift efficiency, H_{SL}, and low H_{sat} suggest efficient spin orbit torque switching is possible. This is confirmed by the direct switching measurements described below.

SOT switching was measured at different H_{long} and current pulse amplitudes to produce switching phase diagrams [Figs. 4(a) and 4(b)]. Magnetization was first set by an out of plane field, then a 1 ms current pulse was applied synchronously with H_{long}. A much smaller current of 25 μA RMS (corresponding to a current density in Pt of about 0.1×10^{10} A/m^2) was applied to sense the direction of the magnetization using a lock-in amplifier after the current pulse. In this measurement, fractional magnetization values between 1 and −1 represent a nonuniform domain state, not a switching probability.[29] The critical switching threshold was taken as the current at which the average magnetization after the current pulse is zero. Figures 4(a) and 4(b) show switching phase diagrams for t_{Au} = 0

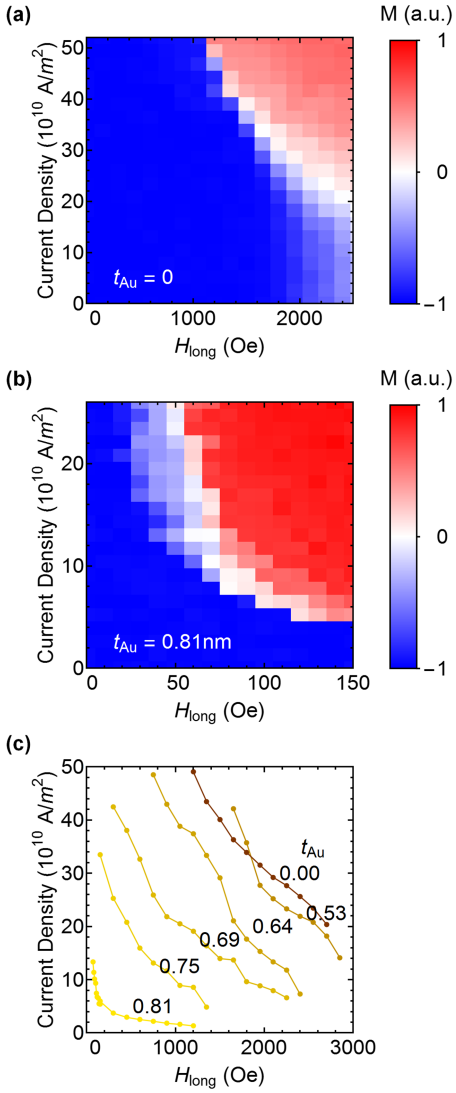

FIG. 4. (a) Switching phase diagram of a sample without a gold spacer layer. (b) Switching phase diagram for t_{Au} = 0.81 nm; note different field and current scales. (c) Comparison of critical switching thresholds for a nearly constant anisotropy set of samples with different t_{Au}, indicated in nm.

and $t_{Au} = 0.81$ nm, respectively. We find that the switching threshold occurs at fields and currents that are about 10 times smaller when the Au layer is present. Figure 4(c) shows switching boundaries for a subset of the nearly constant-anisotropy samples for a range of t_{Au}, revealing a dramatic lowering of the field and current thresholds with increasing t_{Au}.

The decrease in switching current and field are consistent with the change in SOT and DMI, respectively, as measured by the harmonic voltage and hysteresis loop shift. Furthermore, the effects all share the same dependence on the Au thickness, appearing mainly as t_{Au} exceeds 0.5 nm and subsequently scaling somewhat linearly. The insertion of a 0.81 nm gold spacer appears to reduce H_{DMI} about 90%, greatly lowering the in-plane field required for SOT switching. Also appearing at $t_{Au} > 0.5$ nm, spin transport into the ferromagnet doubles according to both the harmonic voltage and hysteresis loop shift.

In conclusion, we found that an ultrathin gold spacer layer inserted at the Pt/Co interface dramatically reduced the DMI and increased the Slonczewski-like SOT effective field, showing that the DMI and the SOT can be engineered independently. The DMI was reduced to such an extent that the H_{long} required for switching might be provided by the exchange bias or stray field from an in-plane magnetized layer. The reductions in both H_{long} and current are relevant to device applications. At the same time, we confirm that, in this heterostructure, the interfacial DMI controls the H_{long} threshold required for SOT switching. We show that the Pt/Co interface is sensitive to an ultrathin spacer layer, which can independently modify the DMI and SOT. A systematic study of various metal spacer layers in bilayer systems with strong spin-orbit coupling may reveal further utility.

This work was supported by the National Science Foundation under NSF-ECCS-1408172. We thank Dr. C. O. Avci for helpful discussions.

[1] C. F. Pai, L. Liu, Y. Li, H. W. Tseng, D. C. Ralph, and R. A. Buhrman, Appl. Phys. Lett. **101**, 122404 (2012).
[2] L. Liu, C.-F. Pai, Y. Li, H. W. Tseng, D. C. Ralph, and R. A. Buhrman, Science **336**, 555 (2012).
[3] L. Liu, O. J. Lee, T. J. Gudmundsen, D. C. Ralph, and R. A. Buhrman, Phys. Rev. Lett. **109**, 096602 (2012).
[4] S. Emori, U. Bauer, S.-M. Ahn, E. Martinez, and G. S. D. Beach, Nat. Mater. **12**, 611 (2013).
[5] I. M. Miron, T. Moore, H. Szambolics, L. D. Buda-Prejbeanu, S. Auffret, B. Rodmacq, S. Pizzini, J. Vogel, M. Bonfim, A. Schuhl, and G. Gaudin, Nat. Mater. **10**, 419 (2011).
[6] I. M. Miron, G. Gaudin, S. Auffret, B. Rodmacq, A. Schuhl, S. Pizzini, J. Vogel, and P. Gambardella, Nat. Mater. **9**, 230 (2010).
[7] B. F. Miao, S. Y. Huang, D. Qu, and C. L. Chien, Phys. Rev. Lett. **111**, 1 (2013).
[8] A. V. Khvalkovskiy, V. Cros, D. Apalkov, V. Nikitin, M. Krounbi, K. A. Zvezdin, A. Anane, J. Grollier, and A. Fert, Phys. Rev. B **87**, 2 (2013).
[9] A. van den Brink, G. Vermijs, A. Solignac, J. Koo, J. T. Kohlhepp, H. J. M. Swagten, and B. Koopmans, Nat. Commun. **7**, 10854 (2015).
[10] S. Fukami, C. Zhang, S. DuttaGupta, A. Kurenkov, and H. Ohno, Nat. Mater. **15**, 535 (2016).
[11] Y.-W. Oh, S. Chris Baek, Y. M. Kim, H. Y. Lee, K.-D. Lee, C.-G. Yang, E.-S. Park, K.-S. Lee, K.-W. Kim, G. Go, J.-R. Jeong, B.-C. Min, H.-W. Lee, K.-J. Lee, and B.-G. Park, Nat. Nanotechnol. **11**, 878 (2016).
[12] Y.-C. Lau, D. Betto, K. Rode, J. Coey, and P. Stamenov, Nat. Nanotechnol. **11**, 758 (2015).
[13] S. A. Razavi, D. Wu, G. Yu, Y. C. Lau, K. L. Wong, W. Zhu, C. He, Z. Zhang, J. M. D. Coey, P. Stamenov, P. K. Amiri, and K. L. Wang, Phys. Rev. Appl. **7**, 024023 (2017).
[14] O. J. Lee, L. Q. Liu, C. F. Pai, Y. Li, H. W. Tseng, P. G. Gowtham, J. P. Park, D. C. Ralph, and R. A. Buhrman, Phys. Rev. B **89**, 024418 (2014).
[15] C. F. Pai, M. Mann, A. J. Tan, and G. S. D. Beach, Phys. Rev. B **93**, 144409 (2016).
[16] J. Kim, J. Sinha, M. Hayashi, M. Yamanouchi, S. Fukami, T. Suzuki, S. Mitani, and H. Ohno, Nat. Mater. **12**, 240 (2013).
[17] M. Hayashi, J. Kim, M. Yamanouchi, and H. Ohno, Phys. Rev. B **89**, 144425 (2014).
[18] C. F. Pai, Y. Ou, L. H. Vilela-Leao, D. C. Ralph, and R. A. Buhrman, Phys. Rev. B **92**, 064426 (2015).
[19] H. Y. Zhang, Y. J. Wang, and G. G. Zheng, IEEE Trans. Magn. **29**, 3376 (1993).
[20] H. Y. Zhang and Y. J. Wang, Acta Phys. Sin. **3**, 780 (1994).
[21] S. Woo, M. Mann, A. J. Tan, L. Caretta, G. S. D. Beach, S. Woo, M. Mann, A. J. Tan, L. Caretta, and G. S. D. Beach, Appl. Phys. Lett. **105**, 212404, (2014).
[22] Y. Tserkovnyak, A. Brataas, G. E. W. Bauer, and B. I. Halperin, Rev. Mod. Phys. **77**, 1375 (2005).
[23] Y. Tserkovnyak, A. Brataas, and G. E. W. Bauer, Phys. Rev. B **66**, 224403 (2002).
[24] C. Du, H. Wang, F. Yang, and P. C. Hammel, Phys. Rev. Appl. **1**, 044004 (2014).
[25] W. Zhang, M. B. Jungfleisch, W. Jiang, Y. Liu, J. E. Pearson, S. G. E. Te Velthuis, A. Hoffmann, F. Freimuth, and Y. Mokrousov, Phys. Rev. B **91**, 115316 (2015).
[26] B. Heinrich, Y. Tserkovnyak, G. Woltersdorf, A. Brataas, R. Urban, and G. E. W. Bauer, Phys. Rev. Lett. **90**, 187601 (2003).
[27] Y. Tserkovnyak, A. Brataas, and G. E. W. Bauer, Phys. Rev. B **67**, 140404 (2003).
[28] S. Emori, E. Martinez, K. J. Lee, H. W. Lee, U. Bauer, S. M. Ahn, P. Agrawal, D. C. Bono, and G. S. D. Beach, Phys. Rev. B **90**, 184427 (2014).
[29] N. Perez, E. Martinez, L. Torres, S. H. Woo, S. Emori, and G. S. D. Beach, Appl. Phys. Lett. **104**, 092403 (2014).